Biogeosciences Discuss., 12, 11891–11934, 2015
www.biogeosciences-discuss.net/12/11891/2015/
doi:10.5194/bgd-12-11891-2015

Biogeosciences
Discussions
Open Access

Sun-induced Chlorophyll fluorescence and PRI improve remote sensing GPP estimates under varying nutrient availability in a typical Mediterranean savanna ecosystem

O. Perez-Priego[1], J. Guan[1,2], M. Rossini[3], F. Fava[3], T. Wutzler[1], G. Moreno[4], N. Carvalhais[1,5], A. Carrara[6], O. Kolle[1], T. Julitta[3], M. Schrumpf[1], M. Reichstein[1], and M. Migliavacca[1]

[1]Max Planck Institute for Biogeochemistry, Biogeochemical Integration department, Jena, Germany
[2]State Key Laboratory of Soil Erosion and Dryland Farming on Loess Plateau, Institute of Soil and Water Conservation, Chinese Academy of Sciences and Ministry of Water Resources, Yangling, Shaanxi 712100, China
[3]Università degli Studi Milano-Bicocca, Remote Sensing of Environmental Dynamics Laboratory, DISAT, Milan, Italy
[4]Universidad de Extremadura, Forest Research Group, Plasencia, 10600, Spain

[5]Departamento de Ciencias e Engenharia do Ambiente, DCEA, Faculdade de Ciencias e Tecnologia, FCT, Universidade Nova de Lisboa, 2829-516 Caparica, Portugal
[6]Fundación Centro de Estudios Ambientales del Mediterráneo (CEAM), Valencia, Spain

Received: 27 May 2015 – Accepted: 5 July 2015 – Published: 30 July 2015

Correspondence to: O. Perez-Priego (opriego@bgc-jena.mpg.de) and M. Migliavacca (mmiglia@bgc-jena.mpg.de)

Published by Copernicus Publications on behalf of the European Geosciences Union.

Abstract

This study investigates the performances of different optical indices to estimate gross primary production (GPP) of herbaceous stratum in a Mediterranean savanna with different Nitrogen (N) and Phosphorous (P) availability. Sun-induced chlorophyll Fluorescence yield computed at 760 nm (Fy760), scaled-photochemical reflectance index (sPRI), MERIS terrestrial-chlorophyll index (MTCI) and Normalized difference vegetation index (NDVI) were computed from near-surface field spectroscopy measurements collected using high spectral resolution spectrometers covering the visible near-infrared regions. GPP was measured using canopy-chambers on the same locations sampled by the spectrometers. We hypothesized that light-use efficiency (LUE) models driven by remote sensing quantities (RSM) can better track changes in GPP caused by nutrient supplies compared to those driven exclusively by meteorological data (MM). Particularly, we compared the performances of different RSM formulations – relying on the use of Fy760 or sPRI as proxy for LUE and NDVI or MTCI as fraction of absorbed photosynthetically active radiation (*f*APAR) – with those of classical MM.

Results showed significantly higher GPP in the N fertilized experimental plots during the growing period. These differences in GPP disappeared in the drying period when senescence effects masked out potential differences due to plant N content. Consequently, although MTCI was tightly related to plant N content ($r^2 = 0.86$, $p < 0.01$), it was poorly related to GPP ($r^2 = 0.45$, $p < 0.05$). On the contrary sPRI and Fy760 correlated well with GPP during the whole measurement period. Results revealed that the relationship between GPP and Fy760 is not unique across treatments but it is affected by N availability. Results from a cross validation analysis showed that MM ($AIC_{cv} = 127$, $ME_{cv} = 0.879$) outperformed RSM ($AIC_{cv} = 140$, $ME_{cv} = 0.8737$) when soil moisture was used to constrain the seasonal dynamic of LUE. However, residual analyses demonstrated that MM is predictively inaccurate whenever no climatic variable explicitly reveals nutrient-related changes in the LUE parameter. These results

put forward that RSM is a valuable means to diagnose nutrient-induced effects on the photosynthetic activity.

1 Introduction

Human-induced nutrient imbalances are affecting essential processes that lead to important changes in ecosystem structure and functioning (Peñuelas et al., 2013). In spite of the crucial role of nutrients in regulating plant processes, efforts to describe and predict the response of photosynthesis to such changes with remote sensing information have been limited. In the framework of the classical Monteith Light Use Efficiency (LUE) model (Monteith, 1972), estimates of photosynthesis (hereafter gross primary productivity, GPP) are based on three key quantities: (i) the fraction of photosynthetically active radiation (fAPAR) absorbed by the vegetation, (ii) potential LUE (or maximum, LUE_m), and (iii) correction factors related to meteorological conditions that limit LUE_m. Although Nitrogen (N) deficiencies have been recognized one of the main controlling factors of LUE_m (Madani et al., 2014), the predictive capability of LUE models is usually circumspect as they operate based on the general assumption that plants are under non-limiting nutrient conditions.

Very little attention has been given to nutrient-induced effects on fAPAR and LUE in common formulations of LUE models. Light absorption by plant is given by chlorophyll pigments that enable photosynthetic processes. Assuming a correlation between leaf chlorophyll pigments and leaf N content, note that N atoms are basic components of the chlorophylls molecular structure, several studies have demonstrated that leaf nitrogen content can be estimated through chlorophyll-related hyperspectral vegetation indices (Baret et al., 2007; Schlemmer et al., 2013). Among these indices, the MERIS Terrestrial Chlorophyll Index (MTCI, Dash and Curran, 2004) has been used as a proxy for fAPAR (Rossini et al., 2010; Wang et al., 2012). However, leaf N content is a trait of GPP not only because it scales with chlorophylls but also regulates enzyme kinetic processes driving photosynthesis and hence the physiological status of the plant (Huang et al., 2004; Walker et al., 2014). Then, prescribing biome-specific LUE parameters and correcting LUE_m only for climatic and environmental conditions may hamper the accurate prediction of GPP (Yuan et al., 2014). For these reasons, recent literature has called for better physiological descriptors of the dynamic behavior of LUE (Guanter et al., 2014).

The sun-induced chlorophyll fluorescence (SIF) or physiological-related reflectance indices such as the photochemical reflectance index (PRI) provide a new optical means to spatially infer LUE (Damm et al., 2010; Guanter et al., 2014; Rossini et al., 2015) and can provide diagnostic information regarding plant nutrient and water status (Lee et al., 2013; Pérez-Priego et al., 2005; Suárez et al., 2008; Tremblay et al., 2012). From a physiological perspective, the efficiency of green plants to transform absorbed light into chemical energy during photosynthesis can be characterized by two main photo-protective mechanisms: (i) non-photochemical quenching that can be detected using the Photochemical Reflectance Index (PRI), originally proposed by (Gamon et al., 1992) to track changes in the de-epoxidation state of the xanthophyll cycle pigments, and (ii) chlorophyll fluorescence, the dissipation of energy that exceeds photosynthetic demand (Krause and Weis, 1984). The PRI has been directly correlated with LUE (Drolet et al., 2008; Gamon et al., 1997; Nichol et al., 2000; Peñuelas et al., 2011; Rahman et al., 2004). However, such relation may vary because of the sensitivity of the PRI to confounding factors like those associated with temporal changes in the relative fraction of chlorophyll : carotenoids pigment composition (Filella et al., 2009; Porcar-Castell et al., 2012), viewing angles and vegetation structure (Garbulsky et al., 2011; Grace et al., 2007; Hall et al., 2008; Hilker et al., 2008).

Alternatively, the estimation of SIF by passive remote sensing systems has been proven feasible in recent years from satellite (Frankenberg et al., 2014; Lee et al., 2013; Parazoo et al., 2014) to the field (Damm et al., 2010; Guanter et al., 2013; Meroni et al., 2011), and opens further possibilities to directly track the dynamics of LUE (Damm et al., 2010; Guanter et al., 2014). Although SIF correlates with LUE, such relations might not be conservative since chlorophyll fluorescence emission varies among species types (Campbell et al., 2008) or with stress conditions such as nutrient deficiencies (Huang et al., 2004; McMurtrey et al., 2003) or drought (Flexas et al., 2002; Pérez-Priego et al., 2005). Likewise with the PRI, the retrieval of SIF from the apparent reflectance signal is not trivial as long as it is affected by the vegetation structure or canopy background components (Zarco-Tejada et al., 2013).

Comparable spatial and temporal resolutions of radiometric and ground-based GPP measurements are essential to accurately optimize LUE model parameters, particularly in heterogeneous ecosystems. Previous studies have related landscape-scale eddy covariance fluxes to radiometric measurements taken in single points to constraint LUE models. However, the explanatory power of GPP models might be greatly reduced by the spatial mismatch between radiometric and eddy covariance flux footprints (Gelybó et al., 2013). Similar issues occur in small-scale factorial experiments where comparable measurements on an intermediate scale between leaf-scale cuvette measurements and landscape-scale eddy covariance measurements are required. Here, we tried to overcome such limitations by combining ground-based radiometric and CO_2 fluxes measurements with similar extension of the measurement footprint using portable spectrometers and canopy chambers in a nutrient-manipulation experiment. The specific objectives were:

a. to assess the effect of different nutrient supplies on grassland photosynthesis and optical properties and their relationships during a phenological cycle, including both growing and drying periods,

b. to evaluate the performance of different LUE modeling approaches with varying nutrient availability and environmental conditions.

2 Material and methods

2.1 Site description and experimental design

A nutrient manipulation experiment was set up in a Mediterranean savannah in Spain (39°56′24.68″ N, 5°45′50.27″ W; Majadas de Tietar, Caceres). The site is characterized by a mean annual temperature of 16 °C, mean annual precipitation of ca. 700 mm, falling mostly from November until May, and by a very dry summer. Similar to most Mediterranean grasland, grazing (< 0.7 cows ha^{-1}) is the main land use in the site. The site is defined as a typical Mediterranean savanna ecosystem, low density of oak trees (mostly *Quercus Ilex* (L.), ~ 20 trees ha^{-1}) dominated by a herbaceous stratum. The experiment itself was restricted to an open grassland area which was not influenced by tree canopy. The herbaceous stratum is dominated by species of the three main functional plant forms (grasses, forbs and legumes). The fraction of the three plant forms varied seasonally according to their phenological status (Table 1). Overall, leaf area measurements of the herbaceous stratum characterized the growing season phenology as peaking early in April and achieving senescence by the end of May (Table 1).

The experiment consisted of four randomized blocks of about 20 m × 20 m. Each block was separated into four plots of 9 m × 9 m with a buffer of 2 m in between to avoid boundary effects. In each block, four treatments were applied (see Fig. 1):

a. control treatment (C) with no fertilization;

b. Nitrogen addition treatment (+N) with an application of 100 kg N ha^{-1} as potassium nitrate (KNO_3) and ammonium nitrate (NH_4NO_3);

c. Phosphorous addition treatment (+P) with an application of 50 kg P ha^{-1} as monopotassium phosphate (KH_2PO_4); and

d. N and P addition treatment (+NP), juxtaposing treatments (b) and (c).

Each fertilizer was dissolved in water and sprayed on foliage early in the growing season (21 March 2014). The same amount of water used in the fertilizer solutions

BGD
12, 11891–11934, 2015

($\sim 2\,L\,m^{-2}$) was sprayed on the C treatment to avoid water imbalances among treatments.

Within each plot, two permanent, non-disturbed parcels (32 in total, see black squares in Fig. 1) were dedicated to monitor CO_2 fluxes (net ecosystem CO_2 exchange, NEE; and daytime ecosystem respiration, R_{eco}). While NEE measurements were performed over the course of the day (from early in the morning to late afternoon), spectral measurements were conducted simultaneously with flux measurements only around noon on half of the parcels (16 in total).

Flux and spectral measurements were carried out in four field campaigns:

- campaign #1: before fertilization (20 March 2014),
- campaign #2: three weeks after fertilization (15 April 2014) during the peak of the growing period,
- campaigns #3 and #4: on 7 and 27 May 2014, respectively, concurring with the drying period were performed to evaluate joint effects related to physiological senescence processes.

Ancillary measurements were taken in every field campaign as follows: green plant area index (PAI_g) and aboveground biomass were directly measured by harvest in four parcels ($0.25\,m \times 0.25\,m$) within each plot in the area surrounding that where spectral and flux measurements were taken. All samples were refrigerated just after collection, and transported for laboratory analyses. Fresh samples were separated into functional groups, the sample was scanned and green plant area was measured using image analysis (WinRHIZO, Regent Instruments Inc., Canada). Afterwards, fresh samples were dried in an oven at 65 °C for 48 h and weighed to determine dry biomass. To analyze the nutrient content in leaf mass, biomass subsamples were ground in a ball mill (RETSCH MM200, Retsch, Haan, Germany) and total C and N concentrations were determined with an elemental analyzer (Vario EL, Elementar, Hanau, Germany). P concentrations were also measured: 100 mg biomass subsamples were diluted in

BGD
12, 11891–11934, 2015

3 mL of HNO_3 65 %, (Merck, Darmstadt, Germany) and microwave digested at high pressure (Multiwave, Anton Paar, Graz, Austria; Raessler et al., 2005). Afterwards, elemental analysis was conducted using inductively coupled plasma – optical emission spectrometry (ICP-OES, Optima 3300 DV, Perkin Elmer, Norwalk, USA).

2.2 Flux measurements and meteorological data

Net CO_2 fluxes were measured with three transparent chambers of a closed dynamic system. The chambers consisted of a cubic (0.6 m × 0.6 m × 0.6 m) transparent low-density polyethylene structure connected to an infrared gas analyzer. The chambers were equipped with different sensors to acquire environmental and soil variables, all installed at the chamber ceiling: photosynthetically active radiation (PAR, placed outside of the chamber to be handled and leveled) was measured with a quantum sensor (Li-190, Li-Cor, Lincoln, NE, USA); air and vegetation temperatures were measured with a thermistor probe (type 107, Campbell Scientific, Logan, Utah, USA) and an infrared thermometer (T_c, IRTS-P, Apogee, UT, USA); atmospheric pressure was measured inside the chamber using a barometric pressure sensor (CS100, Campbell Scientific, Logan, Utah, USA). The chambers were also equipped with soil temperature and humidity sensors; soil water content was determined with an impedance soil moisture probe (Theta Probe ML2x, Delta-T Devices, Cambridge, UK) at 5 cm depth and soil temperature (type 107, Campbell Scientific, Logan, Utah, USA) at 10 cm depth.

The chamber operated as a closed dynamic system. A small pump circulates an air flow of 1 L min^{-1} through the sample circuit: air is drawn from inside the chamber – through three porous-hanging tubes spatially distributed through the chamber headspace – to an infrared gas analyzer (IRGA LI-840, Lincoln, NE, USA), which measures CO_2 and water vapor mole fractions at 1 Hz; this air flow is then returned to the chamber. The hanging tubes allowed spatially distributed sampling, obviating the need to homogenize air during chamber deployment. Nevertheless, one small fan (12 V, 0.14 A) was fixed at 0.3 m on a floor corner of the chamber and angled 45° upward.

A 0.6 m × 0.6 m metal collar was installed in each permanent parcel of each plot. The collar provided a flat surface onto which the bottom of the chamber was placed. The chamber was open and ventilated prior to measurement, so that initial air composition and temperature represented natural atmospheric conditions. For the NEE measurement, the transparent chamber was placed on the collar (closed position), and fluxes were calculated from the rate of change of the CO_2 molar fraction (referenced to dry air) within the chamber. R_{eco} was measured just after NEE using an opaque blanket that covered the entire chamber and kept it dark during the measurements (PAR values around 0). Chamber deployments lasted 3 min as a general rule. Chamber disturbance effects and correction for systematic errors (leakage, water dilution and gas density correction, and light attenuation by the chamber wall) were applied according to Pérez-Priego et al. (2015). Fluxes were calculated with a self-developed R Package (http://r-forge.r-project.org/projects/respchamberproc/).

2.3 Field spectral measurements

Midday spectral measurements at canopy level were carried out under clear sky conditions using two portable spectrometers (HR4000, OceanOptics, USA) characterized by different spectral resolutions. Spectrometer 1, characterized by a Full Width at Half Maximum (FWHM) of 0.1 nm and a 700–800 nm spectral range was specifically designed for the estimation of sun-induced chlorophyll fluorescence at the O_2-A band (760 nm). Spectrometer 2 (FWHM = 1 nm, 400–1000 nm spectral range) was used for the computation of reflectance and vegetation indices. Spectrometers were housed in a thermally regulated Peltier box, keeping the internal temperature at 25 °C in order to reduce dark current drift. The spectrometers were spectrally calibrated with a source of known characteristics (CAL-2000 mercury argon lamp, OceanOptics, USA) while the radiometric calibration was inferred from cross-calibration measurements performed with a calibrated FieldSpec FR Pro spectrometer (ASD, USA). This spectrometer was calibrated by the manufacturer with yearly frequency.

BGD
12, 11891–11934, 2015

Title Page
Abstract Introduction
Conclusions References
Tables Figures
◂ ▸
Back Close
Full Screen / Esc
Printer-friendly Version
Interactive Discussion

Incident solar irradiance was measured by nadir observations of a leveled calibrated standard reflectance panel (Spectralon; LabSphere, USA). Measurements were acquired using bare fiber optics with an angular field of view of 25°. The average canopy plane was observed from nadir at a distance of 110 cm (43 cm diameter field of view) allowing for collecting measurements of 50 % of the surface area covered by the chamber measurements. The manual rotation of a mast mounted horizontally on the tripod allowed sequential observation of the vegetated target and the white reference calibrated panel. More in detail, every acquisition session consisted in the consecutive collection of the following spectra: instrument dark current, radiance of the white reference panel, canopy radiance and radiance of the white reference panel. The radiance of the reference panel at the time of the canopy measurement was then estimated by linear interpolation.

For every acquisition, 3 and 10 scans (for Spectrometers 1 and 2, respectively) were averaged and stored as a single file. Five measurements were collected for each plot. Spectral data were acquired with dedicated software (Meroni and Colombo, 2009) and processed with a specifically developed IDL (ITTVIS IDL 7.1.1) application. This application allowed the basic processing steps of raw data necessary for the computation of the hemispherical conical reflectance factor described by Meroni et al. (2011).

The following indices were selected as suitable to investigate long term nutrient-mediated effects on photosynthesis. The NDVI (Rouse et al., 1974) was selected because it correlates well with plant area and among traditional spectral vegetation indices is used worldwide by classical LUE models as a surrogate for *f*APAR (Di Bella et al., 2004). The MTCI (Dash and Curran, 2004) was selected because it was specifically designed for canopy chlorophyll content estimation, and recently used as proxy for *f*APAR as well as NDVI. In this study we used the PRI and SIF as surrogates for LUE. A scaled PRI (sPRI) calculated as (PRI+1)/2 was used. SIF was estimated by exploiting the spectral fitting method described in Meroni et al. (2010), assuming linear variation of the reflectance and fluorescence in the O_2-A absorption band region. The spectral interval used for SIF estimation was set to 759.00–767.76 nm for a total of 439

BGD
12, 11891–11934, 2015
Remote sensing-based model of photosynthesis
O. Perez-Priego et al.

spectral channels used. For methodological distinction among existing approaches, hereafter SIF is referred to as F760. Because F760 is affected by PAR we use the apparent chlorophyll fluorescence yield (Fy760; Rossini et al., 2010) computed as the ratio between F760 and the incident radiance in a nearby spectral region. A summary of the formulation to compute the vegetation indices and their corresponding target and proxy in the LUE model approach are presented in Table 2.

2.4 Relationship between GPP and remote sensing data

Ecosystem-level GPP was computed as the difference between NEE and daytime R_{eco} taken consecutively with the chambers. To assess how GPP is modulated by light among treatments and over the phenological cycle of the herbaceous stratum, we computed the parameters of photosynthetic light response curve (PLRC). Specifically, the Michaelis–Menten function was fitted to GPP and PAR data taken throughout the day for each field campaign as follows:

$$\mathrm{GPP}_i = \frac{\alpha \cdot \beta \cdot \mathrm{PAR}_i}{\beta + \mathrm{PAR}_i \cdot \alpha} \tag{1}$$

where α is a parameter describing the photosynthetic quantum yield (µmol CO_2 µmol photons^{-1}), and β is the parameter that extrapolates to GPP at saturating light condition (µmol CO_2 m^{-2} s^{-1}). According to Ruimy et al. (1994), we used the optimized parameters of the PLRC as defined in Eq. (1) to estimate the GPP at 2000 µmol quantum m^{-2} s^{-1} of PAR (GPP_{2000}).

We evaluated direct relationships between midday GPP values (measurements taken around noon with the chamber) and simultaneous measurements of Fy760 and spectral indices (NDVI, sPRI, MTCI). In addition, to avoid confounding factors in the relationship between Fy760 and sPRI and photosynthesis, we also used GPP_{2000} as a steady-state photosynthetic capacity descriptor.

BGD
12, 11891–11934, 2015

2.5 Monteith's light-use efficiency modelling approaches

Following Monteith's LUE framework (Eq. 2) two alternative modeling approaches were used:

$$\mathrm{GPP} = \mathrm{LUE} \cdot f\mathrm{APAR} \cdot \mathrm{PAR}, \tag{2}$$

i. Meteorology-driven methods (MM); based on the MOD17 formulation, fAPAR is approached through the relationship with NDVI and includes limiting functions f (meteo), which are based on climatic driving parameters to limit maximum LUE ($\mathrm{LUE}_{\mathrm{max}}$). Alternatively, Eq. (2) was reformulated as follows:

$$\mathrm{GPP} = \mathrm{LUE}_{\mathrm{max}} \cdot f(\mathrm{meteo}) \cdot (a_0 \cdot \mathrm{NDVI} + a_1) \cdot \mathrm{PAR}, \tag{3}$$

where $\mathrm{LUE}_{\mathrm{max}}$, a_o, and a_1 are model parameters. Three different f (meteo) functions were tried;

a. MM-VPD, this method is a simplification of the original MOD17, in which f(meteo) includes two linear ramp functions of both maximum and minimum vapour pressure deficit (VPD) and minimum temperature (T). Since minimum temperature was not limiting at the site, we fixed the f (meteo) parameters as suggested by Heinsch et al. (2006) but constraining only a function based on VPD as follows:

$$f(\mathrm{meteo}) = \left[1 - \left(\frac{\mathrm{VPD} - \mathrm{VPD}_{\mathrm{min}}}{\mathrm{VPD}_{\mathrm{max}} - \mathrm{VPD}_{\mathrm{min}}}\right)\right], \tag{4}$$

then, $\mathrm{VPD}_{\mathrm{max}}$ and $\mathrm{VPD}_{\mathrm{min}}$ are defined as the two parameters of the f(meteo) term.

b. MM-SWC, where f(meteo) includes a soil water content (SWC) function (Migliavacca et al., 2011) as the limiting factor of $\mathrm{LUE}_{\mathrm{max}}$:

$$f(\mathrm{meteo}) = \frac{1}{1 + \exp^{(\mathrm{SWC}_{\mathrm{max}} - a \cdot \mathrm{SWC})}}, \tag{5}$$

BGD
12, 11891–11934, 2015
Remote sensing-based model of photosynthesis
O. Perez-Priego et al.

here, SWC_{max} and a are defined as the parameters of the f(meteo) term.

c. MM (SWC-VPD), where f(meteo) includes both soil water content and VPD functions as limiting factors:

$$f(\text{meteo}) = \left[1 - \left(\frac{\text{VPD} - \text{VPD}_{\text{min}}}{\text{VPD}_{\text{max}} - \text{VPD}_{\text{min}}}\right)\right] \cdot \left[\frac{1}{1 + \exp^{(\text{SWC}_{\text{max}} - a \cdot \text{SWC})}}\right], \tag{6}$$

here, VPD_{max}, VPD_{min}, SWC_{max} and a are defined as the parameters of the f(meteo) term.

ii. RS-based method (RSM); based on a solution of Eq. (1) as follows:

$$\begin{aligned} \text{GPP} &= \text{LUE} \cdot f\text{PAR} \cdot \text{PAR} = (a_0 \cdot \text{Ph} + a_1) \cdot (a_2 \cdot \text{St} + a_3) \cdot \text{PAR} \\ &= (b_0 \cdot \text{Ph} + b_1 \cdot \text{St} + b_2 \cdot \text{Ph} \cdot \text{St} + b_3) \cdot \text{PAR}, \end{aligned} \tag{7}$$

where four alternative model formulations were obtained from the combination of the sPRI or Fy760 as the physiological related proxy (Ph) for LUE, and NDVI or MTCI as structural-related (St) proxy for fAPAR. In Eq. (7), b_0, b_1, b_2, and b_3 are fitting parameters (Rossini et al., 2010).

2.6 Statistical analysis and model performance

All model formulations were optimized using GPP and spectral measurements taken at midday. Since the means of spectral measurements per treatment could have unequal variance, a Welch's t test was performed to evaluate significant differences between the mean values of the different vegetation indices for each treatment and over the four field campaigns. In addition, an analysis of covariance (ANCOVA) was used to test whether or not there was a significant interaction by the treatment effect between GPP and Fy760 and different spectral indices.

2.6.1 Cross validation analyses and model evaluation

Different model formulations were evaluated in leave-one-out (loo) cross-validation: from the whole dataset composed by n observations, one data point at a time was removed. The model was fitted against the $n-1$ remaining data points (training set) while the excluded data (validation set) were used for model evaluation. The cross-validation process was then repeated n times, with each of the n observations used exactly once as the validation set. For each validation set of the cross-validated model, statistics were calculated.

Model accuracy was evaluated by means of different statistics according to Janssen and Heuberger (1995): root mean square error (RMSE), relative root mean square error (rRMSE) determination coefficient (r^2) and model efficiency (ME). The model performances in loo cross-validation were also calculated and reported as RMSE_{cv}, rRMSE_{cv}, r^2 cv and ME_{cv}.

The Akaike Information Criterion (AIC_{cv}) was used to evaluate the trade-off between model complexity (i.e. number of parameters) and explanatory power (i.e. goodness-of-fit) of the different model formulations proposed. The AIC_{cv} is a method based on information theory that is useful for statistical and empirical model selection purposes (Akaike, 1998). Following Anderson et al. (2000), in this analysis we used the following definition of AIC_{cv}:

$$\text{AIC}_{\text{cv}} = 2(\rho + 1) + n\left[\ln\left(\frac{\text{RSS}_{\text{cv}}}{n}\right)\right] \tag{8}$$

where n is the number of samples (i.e. observations), p is the number of model parameters and RSS_{cv} is the residual sum of squares divided by n.

The LUE model formulations proposed in Sect. 2.4 can be ranked according to AIC_{cv}, where the model with lowest AIC_{cv} is considered the best among the different model formulations.

All model parameters (MM, and RSM) were estimated by using a Gauss–Newton nonlinear least square optimization method (Bates and Watts, 2008), and standard

BGD
12, 11891–11934, 2015

errors of parameters were estimated by bootstrapping (number of sampling, $n = 500$; Efron and Tibshirani, 1994), both implemented in the R standard package (R version 3.0.2, R Development Core Team, 2011).

3 Results

3.1 Effects of fertilization on plant nutrient contents and GPP

Fertilization caused strong variations in leaf N and P content among treatments, plant forms and across field campaigns (Table 2); while total N content in plants ranged slightly between 13.8 ± 1.2 and 15.4 ± 1.7 $mg\,g^{-1}$ for the C and +P treatments over the whole experiment, the largest increases in total N were found in the peak of the growing season (#2, 20 March 2014), when +NP and +N treatments reached values of up to 23.7 ± 2.0 and 23.5 ± 4.1 $mg\,g^{-1}$, respectively. Although slightly lower, the differences in total N between C and +P, and +NP and +N remained high over the drying period. P was higher in +NP and +P treatments after fertilization, as compared to +N and C treatments. Consequently, the N : P ratio at the first campaign after fertilization (#2) achieved values of up to 14.2, 6.6, 6, and 3.7, in +N, C, +NP, and +P treatments, respectively. Similar differences in N : P between treatments were also observed during the drying period (#3 and #4, Table 2). On the other hand, PAI_g ranged from 0.4 $m^2\,m^{-2}$ in campaign #4 to up to 2.5 $m^2\,m^{-2}$ in campaign #2. No differences were found in PAI_g among treatments since grazing apparently offset any potential difference in the green aboveground production. Regarding variations in the fraction of plant forms, grass was more abundant in +N and +NP treatments compared to C and +P treatments, particularly during the drying period.

Fertilization caused significant differences in the daily average GPP ($p < 0.05$) between N-addition treatments (mean values of 19.62 ± 4.15 and 18.19 ± 5.67 $\mu mol\,CO_2\,m^{-2}\,s^{-1}$ for +N and +NP, respectively) and C and +P treatments (14.31 ± 5.39 and 14.40 ± 4.09 $\mu mol\,CO_2\,m^{-2}\,s^{-1}$, respectively) in the peak of the growing season (campaign #2); a relative difference of 37 % in GPP was found between +N and +NP and C treatments. During the drying period, however, GPP was substantially down regulated (campaigns #3 and #4) and no significant differences were found, regardless of differences in plant N content observed among treatments. The potential photosynthetic capacity GPP_{2000} (Fig. 2) derived from PLRC was similar in the four treatments in the pretreatment period (campaign #1, Fig. 2a). GPP_{2000} varied throughout the season and peaked in the campaign #2 (15 April) in all treatments. At this time PLRC of the +N and +NP treatments diverged clearly from no N addition treatments (C and +P, Fig. 2b). GPP_{2000} was higher in +N and +NP treatments (18.6 and 20.1 $\mu mol\,CO_2\,m^{-2}\,s^{-1}$, respectively) compared to C and +P treatments (14.9 and 15.4 $\mu mol\,CO_2\,m^{-2}\,s^{-1}$, respectively). After campaign #2, when the soil layer at 5 cm depth dried out appreciably (volumetric water content achieved values of 3 % vol., data not shown), vegetation progressively senesced and GPP in turn was down-regulated and converged to similar values in all treatments, regardless the higher N content observed in +N and +NP treatments as compared with C and +P treatments (Table 2). During the drying season, maximum daily GPP values decreased in all treatments ranging between 7 and 9 $\mu mol\,CO_2\,m^{-2}\,s^{-1}$ and no significant differences between PLRC were observed (Fig. 2c and d). These results indicate that the senescence of the herbaceous stratum, which is regulated by water availability, strongly modulated the photosynthetic capacity of the vegetation over the long term.

3.2 Effects of fertilization on remote sensing data

Optical properties of the analyzed plots were similar during campaign #1, before the nutrient application. A pronounced seasonal time course was observed for both Ph (sPRI and Fy760) and structural indices (St; NDVI and MTCI) with maximum values during the second campaign. It is interesting to note that while for St indices the maximum values were reached in +N plots, +NP plots showed maximum Ph values. Vegetation indices and Fy760 then decreased in the drying period (Fig. 3). As for chamber measurements, differences between treatments were more evident during campaign #2 when C plots showed statistically lower values for all the indices considered, while only MTCI was able to detect significant differences between N fertilized plots (+N and +NP). Furthermore significant differences in Fy760 and MTCI between C and the other three treatments were found ($p < 0.05$) in the drying period (campaign #4,). NDVI varied significantly with changes in PAI_g with values of 0.4 in the campaign #4 up to 0.8 in the campaign #2 ($p < 0.001$, $r^2 = 0.79$).

3.3 Relationship between remote sensing data and GPP

While Ph indices (Fy760 and sPRI) varied linearly with GPP in all treatments ($p < 0.001$, $r^2 = 0.66$ for Fy760 and $p < 0.001$, $r^2 = 0.79$ for sPRI, respectively, Fig. 4a and b), different patterns were observed for St: NDVI and GPP were best fitted by an exponential regression ($p < 0.001$, $r^2 = 0.77$ Fig. 4c), while a weak linear relationship between MTCI and GPP ($p < 0.05$, $r^2 = 0.45$, Fig. 4d) was found. Although a weak relation between MTCI and GPP was found, MTCI was strongly correlated with plant N content ($y = 14.17x - 2.49$, $p < 0.001$, $r^2 = 0.86$). Note that these results are computed excluding data taken in the pre-treatment campaign (#1) and differences in the relationship between remote sensing data and GPP among treatments can be only attributed to nutrient-induced effects. The ANCOVA test did not show significant differences neither in slope nor intercept of the relationship between GPP and sPRI, and NDVI across treatments. However, significant differences were found in the relationship between GPP and Fy760 ($p < 0.1$, Fig. 4b) and GPP and MTCI ($p < 0.01$, Fig. 4d) between N addition treatments (+N and +NP) and C treatments (C and +P).

Similar to GPP, GPP_{2000} was also significantly related to mean midday sPRI ($r^2 = 0.76$, $p < 0.001$, Fig. 5a) and Fy760 ($r^2 = 0.76$, $p < 0.001$, Fig. 5b). As expected, an exponential regression fitted best for NDVI, while a poor relationship with MTCI was found (data not shown).

BGD
12, 11891–11934, 2015

3.4 Modeling GPP

Based on the AIC_{cv} criterion, MM (VPD-SWC) outperformed MM-VPD, MM-SWC and RSM models. Although MM (VPD-SWC) showed high accuracy in the predictions ($ME_{cv} = 0.879$, $r^2_{cv} = 0.881$), this model had a tendency to underestimate observation at high GPP values (see comparison between model predictions and observations, Fig. 6a–c). Note that the highest biases in modeled GPP values among MM models belong to +N and +NP treatments in field campaign #2. Since the four treatments experienced the same environmental conditions (i.e. comparable values of SWC, VPD, air temperature), this bias can be attributed to the higher N content (+N and +NP treatments) as compared to C and +P treatments. Remarkably, residuals of the MM (VPD-SWC) taken from periods with moist soil (SWC > 15) were significantly correlated with sPRI and Fy760 ($p < 0.05$, Fig. 7a and b, respectively). However, no biases between residuals and predictions were observed in RSM over the span of values and treatments (Fig. 8). Results from the evaluation of model performance indicated that RSM performs best when NDVI rather than MTCI, is used as St in the Eq. (7) and, hence, as a proxy for *f*APAR (Table 3). Our results indicated that RSM performs best when either Ph (sPRI or Fy760) is combined with NDVI as St.

4 Discussion

4.1 Effects of nutrients on GPP and remote sensing data and their relationships

Nutrient fertilization, particularly N inputs, induced physiological changes manifested as an increase in photosynthetic capacity (i.e. GPP_{2000}). As we expected, plant N content showed to be a trait of photosynthesis that influences a variety of aspects of photosynthetic physiology (Ciompi et al., 1996; Sugiharto et al., 1990). These physiological changes were reflected on the optical properties, particularly on fluorescence and sPRI. The increase in fluorescence with N fertilization inputs was recently explained as the combined effect that a higher N content has on (1) chlorophyll content, which magnifies APAR and enhances fluorescence signal, and on (2) the increased photosynthetic capacity that increases the fluorescence, that, ultimately reduces the non-photochemical quenching (NPQ), which in turn affects PRI (Cendrero-Mateo et al., 2015).

The relationships between GPP and Fy760 is not unique and may vary from optimal to non-optimal environmental conditions (i.e. nutrient deficiencies, water stress), when other regulatory mechanisms might reduce the degree of coupling between fluorescence and photosynthesis (Cendrero-Mateo et al., 2015; Porcar-Castell et al., 2012). Although Fy760 was positively correlated with GPP, significant differences in the slope of this relationship were observed between treatments (Fig. 4b). Further studies are needed to fully explore the relationship between Fy760 and GPP under different stress conditions and over different ecosystems. However, if confirmed, the effect of nutrient availability on the relationship between Fy760 and GPP could have important implications in GPP modeling. This result suggests that the inclusion of a correction factor related to leaves N : P stoichiometry should be considered when modeling GPP assuming a linear relationship with fluorescence at plant functional type level (Guanter et al., 2014; Joiner et al., 2013).

In this study we also explored the capability of remote sensing to describe ecosystem functional properties defined as those quantities that summarize and integrate ecosystem processes and responses to environmental conditions and can be retrieved from ecosystem level fluxes (e.g. GPP_{2000}) and structural measurements (Reichstein et al., 2014). GPP at light saturation (i.e. GPP_{2000}) is one example of an ecosystem functional property, shown here to be quite correlated to sPRI and Fy760 (Fig. 5). This result suggests that sPRI and Fy760 open also new opportunities for remote sensing products to describe the spatiotemporal variability of essential descriptors of ecosystem functioning. Inferring GPP_{2000} using remote-sensing has important implication both for monitoring global carbon cycle and for benchmarking terrestrial biosphere models.

BGD
12, 11891–11934, 2015
Remote sensing-based model of photosynthesis
O. Perez-Priego et al.

MTCI was tightly related with N content ($r^2 = 0.86$, $p < 0.001$), independent of other structural variables (i.e. PAI_g), and can be used as a good indicator of N availability. Although MTCI has been proven to be very sensitive to variations in chlorophyll contents (Dash and Curran, 2004) and hence linkable with light absorption processes, it was weakly correlated with GPP, particularly in plots added with N (+N and +NP; $r^2 = 0.27$, $p < 0.01$, Fig. 4d). A quite wide range of GPP values were found at high values of MTCI – high GPP values corresponding to the growing season and low ones to the drying period – which can be explained by two simultaneous mechanisms.

First, despite the high plant N content, physiological mechanisms including stomatal control or reduced carboxylation efficiency down-regulate GPP (Huang et al., 2004) and ultimately might break the relationship between GPP and MTCI. Second, MTCI tracks changes in N content regardless changes in canopy structure occuring during the dry season when grass achieved senescence (i.e. green to dry biomass ratio, PAI_g). More studies aimed at the separation of the combined effects of N and changes in green/dry biomass fractions on fAPAR are essential. On the other hand, although NDVI followed the seasonal dynamic of PAIg, it saturated at high GPP values indicating the low ability of this index to detect spatial variations induced by N fertilization.

Although optical measurements were taken at high spatial resolution ($< 0.36\,m^2$), the separation of confounding factors affecting sPRI or Fy760 is essential to elucidate the mechanistic association between sPRI or Fy760 and GPP. Like sPRI, the retrieval of Fy760 from the apparent reflectance signal can be also affected by vegetation structure or canopy background components (Zarco-Tejada et al., 2013). After optimization and selection of the best model parameters using NDVI and sPRI (or Fy760) as driver, we analyzed the response of simulated GPP to variations in NDVI and sPRI (or Fy760, Fig. 9). Results indicate that sPRI explained up to 37.5 % of the relative variations of GPP when NDVI was saturated, particularly at the peak of the growing season (campaign #2) when NDVI was unable to describe changes in GPP. However, when soil dried out during the drying period, and a decrease in photosynthetic capacity was observed, small variations in GPP were hardly explained through sPRI or Fy760 as

BGD
12, 11891–11934, 2015

well (Fig. 9b). Similar to other studies in semi-arid ecosystems, the lack of sensitivity of sPRI or Fy760 to changes in GPP during dry conditions can be explained by the soil background effect on the reflectance signal (Barton and North, 2001; Mänd et al., 2010; Zarco-Tejada et al., 2013). Accordingly, Rahman et al. (2004) pointed out that conditions where sPRI performs best are in dense canopies with low portion of bare soil.

4.2 Performances of different LUE modeling approaches

Here we aim at answering the question how can we better simulate GPP using LUE modeling with varying nutrient availability and environmental conditions by drawing comparisons between the two model philosophies; RSM against MM approaches. There are an increasing number of studies focused on the development of LUE models driven by remotely sensed information to better explain spatio-temporal variations of GPP (Gitelson et al., 2014; Rossini et al., 2012, 2014). However, nutrient availability (and in particular N) greatly influence the spatial variability of LUE even within the same plant-functional type (e.g. grasslands) and further studies are essential. The slightly better performance in cross validation of the MM (VPD-SWC) against all model configurations, including RSM, supports the importance of a joint use of SWC and VPD as key parameters to constraint LUE in arid and semi-arid ecosystems (Prince and Goward, 1995). However, residual analyses demonstrated that MM (VPD-SWC) was unable to track N-induced differences in GPP during the growing period, when both parameters are not limiting (Fig. 7). By contrast, accurate estimates of GPP were obtained with RSM both over the drying and the growing periods. These results also indicate the importance of physiological descriptors to constrain LUE, which prevails over structural factors controlling *f* APAR (i.e. green biomass) under given environmental conditions and encourage the use of hyperspectral remote sensing for diagnostic upscaling of GPP.

With sPRI or Fy760 as a proxy for LUE, RSM is presented as a valuable means to diagnose N-induced effects on physiology. Our results show the limits of MM in predicting the spatial and temporal variability of GPP when LUE is not controlled by meteorological drivers alone (VPD, temperature, soil moisture). Accordingly, GPP is eventually biased whenever neither climatic nor structural state variables explicitly reveal spatial changes in the LUE parameter associated with plant nutrient availability; residuals showed a clear tendency to underestimate the highest modelled GPP values, significantly correlated to Fy760 and sPRI (Fig. 7).

5 Concluding remarks

1. Fy760 and sPRI correlated well with GPP: both increased with N content and decreased with senescence.
2. MTCI can be used as a good descriptor of N content in plants but the relationship with GPP breaks down under drought conditions.
3. Meteo-driven models were able to describe temporal variations in GPP, and soil moisture can be a key parameter to better track the seasonal dynamics of LUE in arid environments. However, meteo-driven models were unable to describe N-induced effects on GPP. Important implication can be derived from these results and uncertainties in the prediction of global GPP still remain when meteo-driven models do not account for plant nutrient availability.
4. sPRI or Fy760 provide valuable means to diagnose nutrient-induced effects on the photosynthetic activity and, therefore, should be included in diagnostic GPP models.

Author contributions. O. Perez-Priego, M. Migliavacca, and M. Rossini conceived the analyses, wrote the introduction, results and discussion, and led the preparation and revision of the manuscript; F. Fava, T. Julitta made hyperspectral measurements, computed spectral indices and fluorescence, and wrote part of the methods section; J. Guan, M. Schrumpf and O. Perez-Priego made chamber measurements, soil and vegetation lab analysis and wrote part of the

BGD
12, 11891–11934, 2015

methods section; J. Guan organized the dataset; O. Kolle provided technical assistance in the design and construction of the chambers and data acquisition system and wrote part of the methods section; G. Moreno and A. Carrara designed the fertilization protocol, organized sampling, provided technical assistance for the managing of the experiment and contributed to data interpretation; T. Wutzler and O. Perez-Priego developed the R package for flux calculations, computed GPP and flux uncertainties and contributed to statistical analyses and interpretation. N. Carvalhais and M. Reichstein contributed to analyses and interpretation and to draft the manuscript. All authors discussed the results and contributed to the manuscript.

Acknowledgements. The authors acknowledge the Alexander von Humboldt Foundation and the Max Planck Research Award that is funding the research activity. We acknowledge City council of Majadas de Tietar for its support. The authors acknowledge Andrea Perez-Bargueno, and Enrique Juarez-Alcalde from (University of Extreamdura), Ramon Lopez-Jimenez (CEAM), Kathrin Henkel, and Martin Hertel from (MPI-Jena) and Marco Celesti (UNIMIB) for the support in the field, lab analysis and the development of the transparent chambers; Javier Pacheco Labrador and Maria Pilar Isabel Martin (CSIC) for help calibrating the radiometric system. We thank Andrew S. Kowalski (University of Granada, Spain) for his review of the manuscript and constructive comments.

The article processing charges for this open-access publication were covered by the Max Planck Society.

References

Akaike, H.: Information theory and an extension of the maximum likelihood principle, in: Selected Papers of Hirotugu Akaike, edited by: Parzen, E., Tanabe, K., and Kitagawa, G., Springer Series in Statistics, Springer, New York, 199–213, 1998.

Anderson, D. R., Burnham, K. P., and Thompson, W. L.: Null hypothesis testing: problems, prevalence, and an alternative, J. Wildlife Manage., 64, 912–923, 2000.

Baret, F., Houlès, V., and Guérif, M.: Quantification of plant stress using remote sensing observations and crop models: the case of nitrogen management, J. Exp. Bot., 58, 869–880, 2007.

BGD

12, 11891–11934, 2015

Barton, C. V. M. and North, P. R. J.: Remote sensing of canopy light use efficiency using the photochemical reflectance index: model and sensitivity analysis, Remote Sens. Environ., 78, 264–273, 2001.
Bates, D. M. and Watts, D. G.: Frontmatter, in: Nonlinear Regression Analysis and Its Applications, John Wiley & Sons, Inc., Hoboken, NJ, USA, 40–43, 2008.
Campbell, P. K. E., Middleton, E. M., Corp, L. A., and Kim, M. S.: Contribution of chlorophyll fluorescence to the apparent vegetation reflectance, Sci. Total Environ., 404, 433–439, 2008.
Cendrero-Mateo, M. P., Carmo-Silva, A. E., Porcar-Castell, A., Hamerlynck, E. P., Papuga, S. A., and Moran, M. S.: Dynamic response of plant chlorophyll fluorescence to light, water and nutrient availability, Funct. Plant Biol., 42, 746–757, doi:10.1071/FP15002, 2015.
Ciompi, S., Gentili, E., Guidi, L., and Soldatini, G. F.: The effect of nitrogen deficiency on leaf gas exchange and chlorophyll fluorescence parameters in sunflower, Plant Sci., 118, 177–184, 1996.
Damm, A., Elbers, J., Erler, A., Gioli, B., Hamdi, K., Hutjes, R., Kosvancova, M., Meroni, M., Miglietta, F., Moersch, A., Moreno, J., Schickling, A., Sonnenschein, R., Udelhoven, T., van der Linden, S., Hostert, P., and Rascher, U.: Remote sensing of sun-induced fluorescence to improve modeling of diurnal courses of gross primary production (GPP), Glob. Change Biol., 16, 171–186, 2010.
Dash, J. and Curran, P. J.: The MERIS terrestrial chlorophyll index, Int. J. Remote Sens., 25, 5403–5413, 2004.
Di Bella, C. M., Paruelo, J. M., Becerra, J. E., Bacour, C., and Baret, F.: Effect of senescent leaves on NDVI-based estimates of *f* APAR: experimental and modelling evidences, Int. J. Remote Sens., 25, 5415–5427, 2004.
Drolet, G. G., Middleton, E. M., Huemmrich, K. F., Hall, F. G., Amiro, B. D., Barr, A. G., Black, T. A., McCaughey, J. H., and Margolis, H. A.: Regional mapping of gross light-use efficiency using MODIS spectral indices, Remote Sens. Environ., 112, 3064–3078, 2008.
Efron, B. and Tibshirani, R. J.: An Introduction to the Bootstrap, CRC Monographs on Statistics & Applied Probability, Chapman & Hall, New York, 271–281, 1994.
Filella, I., Porcar-Castell, A., Munné-Bosch, S., Bäck, J., Garbulsky, M. F., and Peñuelas, J.: PRI assessment of long-term changes in carotenoids/chlorophyll ratio and short-term changes in de-epoxidation state of the xanthophyll cycle, Int. J. Remote Sens., 30, 4443–4455, 2009.
Flexas, J., Escalona, J. M., Evain, S., Gulías, J., Moya, I., Osmond, C. B., and Medrano, H.: Steady-state chlorophyll fluorescence (Fs) measurements as a tool to follow variations of

BGD
12, 11891–11934, 2015

Remote sensing-based model of photosynthesis

O. Perez-Priego et al.

net CO_2 assimilation and stomatal conductance during water-stress in C_3 plants, Physiol. Plantarum, 114, 231–240, 2002.
Frankenberg, C., O'Dell, C., Berry, J., Guanter, L., Joiner, J., Köhler, P., Pollock, R., and Taylor, T. E.: Prospects for chlorophyll fluorescence remote sensing from the Orbiting Carbon Observatory-2, Remote Sens. Environ., 147, 1–12, 2014.
Gamon, J. A., Peñuelas, J., and Field, C. B.: A narrow-waveband spectral index that tracks diurnal changes in photosynthetic efficiency, Remote Sens. Environ., 41, 35–44, 1992.
Gamon, J. A., Serrano, L., and Surfus, J. S.: The photochemical reflectance index: an optical indicator of photosynthetic radiation use efficiency across species, functional types, and nutrient levels, Oecologia, 112, 492–501, 1997.
Garbulsky, M. F., Peñuelas, J., Gamon, J., Inoue, Y., and Filella, I.: The photochemical reflectance index (PRI) and the remote sensing of leaf, canopy and ecosystem radiation use efficiencies: a review and meta-analysis, Remote Sens. Environ., 115, 281–297, 2011.
Gelybó, G., Barcza, Z., Kern, A., and Kljun, N.: Effect of spatial heterogeneity on the validation of remote sensing based GPP estimations, Agr. Forest Meteorol., 174–175, 43–53, 2013.
Gitelson, A. A., Peng, Y., Arkebauer, T. J., and Schepers, J.: Relationships between gross primary production, green LAI, and canopy chlorophyll content in maize: implications for remote sensing of primary production, Remote Sens. Environ., 144, 65–72, 2014.
Grace, J., Nichol, C., Disney, M., Lewis, P., Quaife, T., and Bowyer, P.: Can we measure terrestrial photosynthesis from space directly, using spectral reflectance and fluorescence?, Glob. Change Biol., 13, 1484–1497, 2007.
Guanter, L., Rossini, M., Colombo, R., Meroni, M., Frankenberg, C., Lee, J.-E., and Joiner, J.: Using field spectroscopy to assess the potential of statistical approaches for the retrieval of sun-induced chlorophyll fluorescence from ground and space, Remote Sens. Environ., 133, 52–61, 2013.
Guanter, L., Zhang, Y., Jung, M., Joiner, J., Voigt, M., Berry, J. A., Frankenberg, C., Huete, A. R., Zarco-Tejada, P., Lee, J.-E., Moran, M. S., Ponce-Campos, G., Beer, C., Camps-Valls, G., Buchmann, N., Gianelle, D., Klumpp, K., Cescatti, A., Baker, J. M., and Griffis, T. J.: Global and time-resolved monitoring of crop photosynthesis with chlorophyll fluorescence, P. Natl. Acad. Sci. USA, 111, E1327–E1333, 2014.
Hall, F. G., Hilker, T., Coops, N. C., Lyapustin, A., Huemmrich, K. F., Middleton, E., Margolis, H., Drolet, G., and Black, T. A.: Multi-angle remote sensing of forest light use efficiency by ob-

serving PRI variation with canopy shadow fraction, Remote Sens. Environ., 112, 3201–3211, 2008.

Heinsch, F. A., Maosheng, Z., Running, S. W., Kimball, J. S., Nemani, R. R., Davis, K. J., Bolstad, P. V., Cook, B. D., Desai, A. R., Ricciuto, D. M., Law, B. E., Oechel, W. C., Hyojung, K., Hongyan, L., Wofsy, S. C., Dunn, A. L., Munger, J. W., Baldocchi, D. D., Liukang, X., Hollinger, D. Y., Richardson, A. D., Stoy, P. C., Siqueira, M. B. S., Monson, R. K., Burns, S. P., and Flanagan, L. B.: Evaluation of remote sensing based terrestrial productivity from MODIS using regional tower eddy flux network observations, IEEE T. Geosci. Remote, 44, 1908–1925, 2006.

Hilker, T., Coops, N. C., Hall, F. G., Black, T. A., Wulder, M. A., Nesic, Z., and Krishnan, P.: Separating physiologically and directionally induced changes in PRI using BRDF models, Remote Sens. Environ., 112, 2777–2788, 2008.

Huang, Z. A., Jiang, D. A., Yang, Y., Sun, J. W., and Jin, S. H.: Effects of nitrogen deficiency on gas exchange, chlorophyll fluorescence, and antioxidant enzymes in leaves of rice plants, Photosynthetica, 42, 357–364, 2004.

Janssen, P. H. M. and Heuberger, P. S. C.: Calibration of process-oriented models, Ecol. Model., 83, 55–66, 1995.

Joiner, J., Guanter, L., Lindstrot, R., Voigt, M., Vasilkov, A. P., Middleton, E. M., Huemmrich, K. F., Yoshida, Y., and Frankenberg, C.: Global monitoring of terrestrial chlorophyll fluorescence from moderate-spectral-resolution near-infrared satellite measurements: methodology, simulations, and application to GOME-2, Atmos. Meas. Tech., 6, 2803–2823, doi:10.5194/amt-6-2803-2013, 2013.

Krause, G. H. and Weis, E.: Chlorophyll fluorescence as a tool in plant physiology, Photosynth. Res., 5, 139–157, 1984.

Lee, J.-E., Frankenberg, C., van der Tol, C., Berry, J. A., Guanter, L., Boyce, C. K., Fisher, J. B., Morrow, E., Worden, J. R., Asefi, S., Badgley, G., and Saatchi, S.: Forest productivity and water stress in Amazonia: observations from GOSAT chlorophyll fluorescence, P. Roy. Soc. B-Biol. Sci., 280, 20130171, doi:10.1098/rspb.2013.0171, 2013.

Madani, N., Kimball, J. S., Affleck, D. L. R., Kattge, J., Graham, J., van Bodegom, P. M., Reich, P. B., and Running, S. W.: Improving ecosystem productivity modeling through spatially explicit estimation of optimal light use efficiency, J. Geophys. Res.-Biogeo., 119, 1755–1769, 2014.

BGD

12, 11891–11934, 2015

Mänd, P., Hallik, L., Peñuelas, J., Nilson, T., Duce, P., Emmett, B. A., Beier, C., Estiarte, M., Garadnai, J., Kalapos, T., Schmidt, I. K., Kovács-Láng, E., Prieto, P., Tietema, A., Westerveld, J. W., and Kull, O.: Responses of the reflectance indices PRI and NDVI to experimental warming and drought in European shrublands along a north–south climatic gradient, Remote Sens. Environ., 114, 626–636, 2010.

McMurtrey, J. E., Middleton, E. M., Corp, L. A., Campbell, P., Butcher, L. M., and Daughtry, C. S. T.: Optical reflectance and fluorescence for detecting nitrogen needs in *Zea mays* L., Geoscience and Remote Sensing Symposium, IGARSS '03, 21–25 July 2003, Proceedings, IEEE International , vol.7, 4602–4604, doi:10.1109/IGARSS.2003.1295594, 2003.

Meroni, M. and Colombo, R.: 3S: a novel program for field spectroscopy, Comput. Geosci., 35, 1491–1496, 2009.

Meroni, M., Busetto, L., Colombo, R., Guanter, L., Moreno, J., and Verhoef, W.: Performance of spectral fitting methods for vegetation fluorescence quantification, Remote Sens. Environ., 114, 363–374, 2010.

Meroni, M., Barducci, A., Cogliati, S., Castagnoli, F., Rossini, M., Busetto, L., Migliavacca, M., Cremonese, E., Galvagno, M., Colombo, R., and di Cella, U. M.: The hyperspectral irradiometer, a new instrument for long-term and unattended field spectroscopy measurements, Rev. Sci. Instrum., 82, 043106, doi:10.1063/1.3574360, 2011.

Migliavacca, M., Galvagno, M., Cremonese, E., Rossini, M., Meroni, M., Sonnentag, O., Cogliati, S., Manca, G., Diotri, F., Busetto, L., Cescatti, A., Colombo, R., Fava, F., Morra di Cella, U., Pari, E., Siniscalco, C., and Richardson, A. D.: Using digital repeat photography and eddy covariance data to model grassland phenology and photosynthetic CO_2 uptake, Agr. Forest Meteorol., 151, 1325–1337, 2011.

Monteith, J. L.: Solar radiation and productivity in tropical ecosystems, J. Appl. Ecol., 9, 747–766, 1972.

Nichol, C. J., Huemmrich, K. F., Black, T. A., Jarvis, P. G., Walthall, C. L., Grace, J., and Hall, F. G.: Remote sensing of photosynthetic-light-use efficiency of boreal forest, Agr. Forest Meteorol., 101, 131–142, 2000.

Parazoo, N. C., Bowman, K., Fisher, J. B., Frankenberg, C., Jones, D. B. A., Cescatti, A., Pérez-Priego, Ó., Wohlfahrt, G., and Montagnani, L.: Terrestrial gross primary production inferred from satellite fluorescence and vegetation models, Glob. Change Biol., 20, 3103–3121, 2014.

Peñuelas, J., Garbulsky, M. F., and Filella, I.: Photochemical reflectance index (PRI) and remote sensing of plant CO_2 uptake, New Phytol., 191, 596–599, 2011.
Peñuelas, J., Poulter, B., Sardans, J., Ciais, P., van der Velde, M., Bopp, L., Boucher, O., Godderis, Y., Hinsinger, P., Llusia, J., Nardin, E., Vicca, S., Obersteiner, M., and Janssens, I. A.: Human-induced nitrogen–phosphorus imbalances alter natural and managed ecosystems across the globe, Nature Communications, 4, 2934, doi:10.1038/ncomms3934, 2013.
Pérez-Priego, O., Zarco-Tejada, P. J., Miller, J. R., Sepulcre-Cantó, G., and Fereres, E.: Detection of water stress in orchard trees with a high-resolution spectrometer through chlorophyll fluorescence in-filling of the O_2-A band, IEEE T. Geosci. Remote, 43, 2860–2868, 2005.
Pérez-Priego, O., López-Ballesteros, A., Sánchez-Cañete, E., Serrano-Ortiz, P., Kutzbach, L., Domingo, F., Eugster, W., and Kowalski, A.: Analysing uncertainties in the calculation of fluxes using whole-plant chambers: random and systematic errors, Plant Soil, 1–16, doi:10.1007/s11104-015-2481-x, 2015.
Porcar-Castell, A., Garcia-Plazaola, J., Nichol, C., Kolari, P., Olascoaga, B., Kuusinen, N., Fernández-Marín, B., Pulkkinen, M., Juurola, E., and Nikinmaa, E.: Physiology of the seasonal relationship between the photochemical reflectance index and photosynthetic light use efficiency, Oecologia, 170, 313–323, 2012.
Prince, S. D. and Goward, S. N.: Global primary production: a remote sensing approach, J. Biogeogr., 22, 815–835, 1995.
Raessler, M., Rothe, J., and Hilke, I.: Accurate determination of Cd, Cr, Cu and Ni in woodlice and their skins – is moulting a means of detoxification?, Sci. Total Environ., 337, 83–90, 2005.
Rahman, A. F., Cordova, V. D., Gamon, J. A., Schmid, H. P., and Sims, D. A.: Potential of MODIS ocean bands for estimating CO_2 flux from terrestrial vegetation: a novel approach, Geophys. Res. Lett., 31, L10503, doi:10.1029/2004GL019778, 2004.
Reichstein, M., Bahn, M., Mahecha, M. D., Kattge, J., and Baldocchi, D. D.: Linking plant and ecosystem functional biogeography, P. Natl. Acad. Sci. USA, 111, 13697–13702, 2014.
Rossini, M., Meroni, M., Migliavacca, M., Manca, G., Cogliati, S., Busetto, L., Picchi, V., Cescatti, A., Seufert, G., and Colombo, R.: High resolution field spectroscopy measurements for estimating gross ecosystem production in a rice field, Agr. Forest Meteorol., 150, 1283–1296, 2010.
Rossini, M., Cogliati, S., Meroni, M., Migliavacca, M., Galvagno, M., Busetto, L., Cremonese, E., Julitta, T., Siniscalco, C., Morra di Cella, U., and Colombo, R.: Remote sensing-based esti-

BGD
12, 11891–11934, 2015

Remote sensing-based model of photosynthesis

O. Perez-Priego et al.

mation of gross primary production in a subalpine grassland, Biogeosciences, 9, 2565–2584, doi:10.5194/bg-9-2565-2012, 2012.

Rossini, M., Migliavacca, M., Galvagno, M., Meroni, M., Cogliati, S., Cremonese, E., Fava, F., Gitelson, A., Julitta, T., Morra di Cella, U., Siniscalco, C., and Colombo, R.: Remote estimation of grassland gross primary production during extreme meteorological seasons, Int. J. Appl. Earth Obs., 29, 1–10, 2014.

Rossini, M., Nedbal, L., Guanter, L., Ač, A., Alonso, L., Burkart, A., Cogliati, S., Colombo, R., Damm, A., Drusch, M., Hanus, J., Janoutova, R., Julitta, T., Kokkalis, P., Moreno, J., Novotny, J., Panigada, C., Pinto, F., Schickling, A., Schüttemeyer, D., Zemek, F., and Rascher, U.: Red and far red Sun-induced chlorophyll fluorescence as a measure of plant photosynthesis, Geophys. Res. Lett., 42, 1632–1639, 2015.

Rouse, J. W., Haas, R. H., Schell, J. A., Deering, D. W., and Harlan, J. C.: Monitoring the Vernal Advancements and Retro Gradation of Natural Vegetation, E74-10676, NASA-CR-139243, PR-7, Greenbelt, MD, USA, 1974.

Ruimy, A., Saugier, B., and Dedieu, G.: Methodology for the estimation of terrestrial net primary production from remotely sensed data, J. Geophys. Res., 99, 5263–5283, 1994.

Schlemmer, M., Gitelson, A., Schepers, J., Ferguson, R., Peng, Y., Shanahan, J., and Rundquist, D.: Remote estimation of nitrogen and chlorophyll contents in maize at leaf and canopy levels, Int. J. Appl. Earth Obs., 25, 47–54, 2013.

Suárez, L., Zarco-Tejada, P. J., Sepulcre-Cantó, G., Pérez-Priego, O., Miller, J. R., Jiménez-Muñoz, J. C., and Sobrino, J.: Assessing canopy PRI for water stress detection with diurnal airborne imagery, Remote Sens. Environ., 112, 560–575, 2008.

Sugiharto, B., Miyata, K., Nakamoto, H., Sasakawa, H., and Sugiyama, T.: Regulation of expression of carbon-assimilating enzymes by nitrogen in maize leaf, Plant Physiol., 92, 963–969, 1990.

Tremblay, N., Wang, Z., and Cerovic, Z.: Sensing crop nitrogen status with fluorescence indicators. A review, Agron. Sustain. Dev., 32, 451–464, 2012.

Walker, A. P., Beckerman, A. P., Gu, L., Kattge, J., Cernusak, L. A., Domingues, T. F., Scales, J. C., Wohlfahrt, G., Wullschleger, S. D., and Woodward, F. I.: The relationship of leaf photosynthetic traits – Vcmax and Jmax – to leaf nitrogen, leaf phosphorus, and specific leaf area: a meta-analysis and modeling study, Ecology and Evolution, 4, 3218–3235, 2014.

Wang, W., Yao, X., Yao, X., Tian, Y., Liu, X., Ni, J., Cao, W., and Zhu, Y.: Estimating leaf nitrogen concentration with three-band vegetation indices in rice and wheat, Field Crop. Res., 129, 90–98, 2012.
Yuan, W., Cai, W., Liu, S., Dong, W., Chen, J., Arain, M. A., Blanken, P. D., Cescatti, A., Wohlfahrt, G., Georgiadis, T., Genesio, L., Gianelle, D., Grelle, A., Kiely, G., Knohl, A., Liu, D., Marek, M. V., Merbold, L., Montagnani, L., Panferov, O., Peltoniemi, M., Rambal, S., Raschi, A., Varlagin, A., and Xia, J.: Vegetation-specific model parameters are not required for estimating gross primary production, Ecol. Model., 292, 1–10, 2014.
Zarco-Tejada, P. J., Suarez, L., and Gonzalez-Dugo, V.: Spatial resolution effects on chlorophyll fluorescence retrieval in a heterogeneous canopy using hyperspectral imagery and radiative transfer simulation, IEEE Geosci. Remote S., 10, 937–941, 2013.

BGD
12, 11891–11934, 2015

Remote sensing-based model of photosynthesis

O. Perez-Priego et al.

BGD

12, 11891–11934, 2015

Remote sensing-based model of photosynthesis

O. Perez-Priego et al.

Table 1. Ancillary data resulting from the analysis. Green Plant Area Index (PAIg), fraction of PAI in different plant forms (fPAI), and C, N, and P plant content. The N : P ratio also is shown. Data correspond to the mean value and standard deviation (SD) of the subsamples taken in each plot and treatment.

Campaign Date	Treatment –	Total PAIg ($m^2 m^{-2}$) mean ± SD	Forbs f_{PAI} %	Grass f_{PAI} %	legumes f_{PAI} %	Total C content ($mg\,g^{-1}$) mean ± SD	Total N content ($mg\,g^{-1}$) mean ± SD	Total P content ($mg\,g^{-1}$) mean ± SD	N/P ($mg\,g^{-1}$) –
#1 20 Mar 2014	C	0.85 ± 0.18	28.6 ± 5.2	65.8 ± 8	5.6 ± 3	425	17.7	2.08	8.5
Growing period	N	0.76 ± 0.21	30.6 ± 11.1	63.35 ± 11.3	10.2 ± 9.4	463	18.6	1.99	9.34
Pre-treatment	NP	1.03 ± 0.3	26.4 ± 8.7	63.3 ± 11.3	10.2 ± .9.4	421	18.1	1.90	9.52
	P	0.95 ± 0.21	22.8 ± 8.4	71 ± 7.4	6.2 ± 3.1	369	16.9	1.94	8.71
#2 15 Apr 2014	C	2.02 ± 0.43	23.1 ± 4.2	74.2 ± 3.2	2.7 ± 1.7	413 ± 152	14.6 ± 0.8	2.23 ± 0.02	6.6
Growing period	N	2.17 ± 0.91	20.4 ± 15.2	76.4 ± 18	3.2 ± 2.8	384 ± 121	23.7 ± 2	1.68 ± 0.03	14.2
Post-treatment	NP	2.46 ± 0.45	14.3 ± 10.3	81.1 ± 9.5	4.7 ± 5.8	377 ± 330	23.5 ± 4.1	3.95 ± 0.04	6.0
	P	1.66 ± 0.58	19.5 ± 14.4	77.5 ± 15.4	3.1 ± 2.3	394 ± 212	15.4 ± 1.7	4.22 ± 0.06	3.7
#3 7 May 2014	C	1.08 ± 0.27	29.9 ± 10.3	68.4 ± 10.2	1.7 ± 1.9	447 ± 52	14.2 ± 1.3	2.41 ± 0.02	5.9
Dry period	N	1.29 ± 0.58	18.9 ± 15.6	79.7 ± 16.5	1.4 ± 1.1	449 ± 114	20.1 ± 3.1	1.86 ± 0.03	10.8
	NP	0.84 ± 0.21	17.5 ± 3.7	81.1 ± 4.8	1.5 ± 1.4	438 ± 64	20.6 ± 1.2	3.50 ± 0.04	5.9
	P	1.37 ± 0.57	22.7 ± 11.5	75.9 ± 10.5	1.5 ± 2.2	444 ± 206	14.7 ± 0.8	3.83 ± 0.03	3.8
#4 27 May 2014	C	0.44 ± 0.10	73.3 ± 15	26.5 ± 15.3	0.2 ± 0.5	442 ± 2	13.8 ± 1.2	2.12 ± 0.01	6.5
Dry period	N	0.48 ± 0.28	67.9 ± 28	32.1 ± 28	0.0	448 ± 3	19.0 ± 2.8	1.93 ± 0.02	9.8
	NP	0.53 ± 0.26	70.1 ± 17.2	29.8 ± 17.3	0.1 ± 0.1	442 ± 1	18.5 ± 3.4	2.63 ± 0.02	7.1
	P	0.71 ± 0.31	67.1 ± 17.1	32.4 ± 17.5	0.5 ± 0.4	441 ± 72	13.2 ± 0.7	2.62 ± 0.02	5.0

Table 2. Spectral vegetation indices computed in this study. Vegetation indices are classified into two major classes based on their suitability in inferring fAPAR (structural related indices) and LUE (physiologically-related indices) parameters. R denotes the reflectance at the specified wavelength (nm). NDVI: normalized difference vegetation index; MTCI: MERIS terrestrial chlorophyll index; NDI: normalized difference index; sPRI: scaled Photochemical Reflectance Index; Fy760: apparent fluorescence yield at 760 nm.

Index	Target	Model proxy	Formulation	References
NDVI	Green biomass and leaf area	f_{APAR}	$(R_{800} - R_{680})/(R_{800} + R_{680})$	Rouse et al. (1974)
MTCI	Chlorophyll and nitrogen content	f_{APAR}	$(R_{754} - R_{709})/(R_{709} - R_{681})$	Dash and Curran (2004)
sPRI	Physiology	LUE	$(R_{531} - R_{570})/(R_{531} + R_{570})$	Gamon et al. (1992)
Fy_{760}	Physiology	LUE	Chlorophyll fluorescence in-filling of the O_2-A band	Meroni and Colombo (2006)

BGD
12, 11891–11934, 2015

Remote sensing-based model of photosynthesis

O. Perez-Priego et al.

Table 3. Results from the model evaluation one leave out cross validation analysis across LUE model configurations and vegetation indices. Based on AICcv, the best performance among formulation test for each method is highlighted text bold.

LUE Model	Variable	RMSE (μmol CO_2 m^{-2} s^{-1})	rRMSE	r2	ME	RMSEcv (μmol CO_2 m^{-2} s^{-1})	rRMSEcv	r2cv	MEcv	AICcv
MM-VPD	NDVI	3.041	23.439	0.894	0.802	3.143	24.671	0.877	0.788	160.887
MM-SWC	NDVI	2.663	32.909	0.849	0.848	2.769	34.840	0.835	0.829	148.417
MM (VPD-SWC)	**NDVI**	**2.230**	**21.727**	**0.894**	**0.893**	**2.357**	**23.266**	**0.881**	**0.879**	**127.478**
RSM	**PRI-NDVI**	**2.390**	**24.112**	**0.879**	**0.877**	**2.760**	**30.832**	**0.844**	**0.837**	**140.627**
RSM	PRI-MTCI	3.113	35.793	0.794	0.792	3.489	42.123	0.751	0.739	171.125
RSM	**Fy760-NDVI**	**2.490**	**27.743**	**0.868**	**0.867**	**2.835**	**34.242**	**0.834**	**0.828**	**144.116**
RSM	Fy760-MTCI	3.676	46.770	0.710	0.710	4.074	52.224	0.654	0.644	191.275

BGD
12, 11891–11934, 2015

Table 4. Abbreviations.

a, a_o, and a_1	are model parameters
b_0, b_1, b_2, and b_3	are fitting parameters of RSM
EFPs	ecosystem functional properties
f(meteo)	limiting functions relying on meteorologically-driven data
fAPAR	fraction of absorbed photosynthetically active radiation
fPAIg	fraction of PAIg in different plant forms
Fy760	sun-induced chlorophyll Fluorescence yield at 760 nm
GPP	gross primary productivity
GPP_{2000}	gross primary productivity estimated at 2000 of PAR
LUE	light use-efficiency
LUE_m	potential or maximum LUE
MM	meteorologically driven model
MM-VPD	simplifier model of the original MOD17 that account for VPD in f(meteo)
MM(SWC-VPD)	meteorologically-driven model that account for VPD and soil moisture in f(meteo)
MTCI	MERIS terrestrial-chlorophyll index
NDVI	Normalized difference vegetation index
NEE	net ecosystem CO_2 exchange
PAIg	Green Plant Area Index
PAR	Photosynthetically active radiation
ph	physiologically-related parameter of RSM referring to either sPRI or Fy760 as a proxy for LUE
PLRC	photosynthetic light response curve
PRI	photochemical reflectance index
R_{eco}	daytime ecosystem respiration
RSM	remote sensing based models
SIF	sun-induced chlorophyll fluorescence
sPRI	scaled-photochemical reflectance index
st	structurally-related parameter of RSM referring to either NDVI or MTCI as a proxy for fAPAR
SWC	soil water content
SWC_{max}	parameter of the f(meteo) term
VPD	vapor pressure deficit
VPD_{max} and VPD_{min}	are fitting parameters of the f(meteo) term
α	is a parameter describing the photosynthetic quantum yield
β	is the parameter that extrapolates to GPP at saturating light condition

BGD
12, 11891–11934, 2015

Remote sensing-based model of photosynthesis

O. Perez-Priego et al.

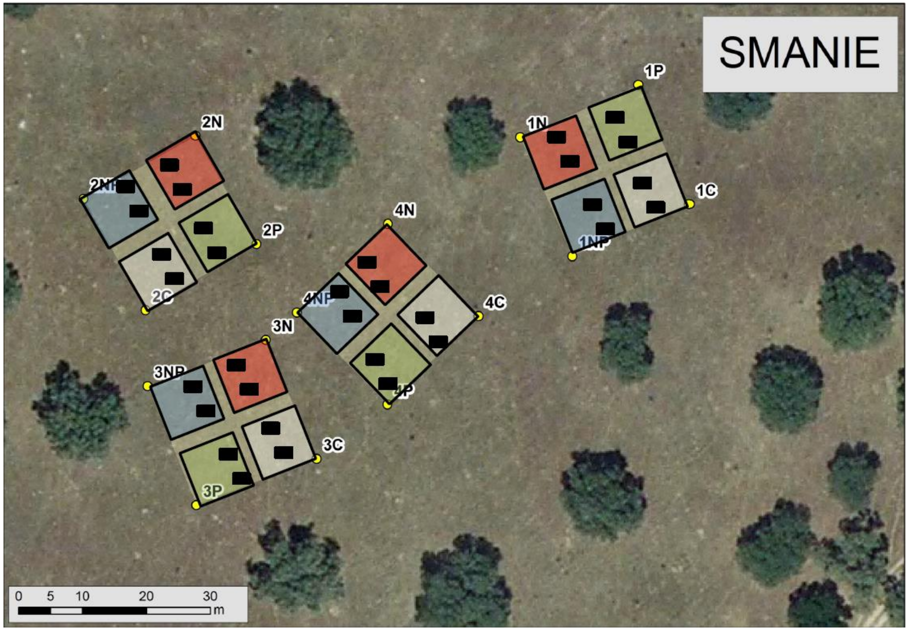

Figure 1. Overview of the experimental site (SMANIE): the experimental blocks are drawn on an image acquired with the hyperspectral AHS (Sensytech Inc., Beverly, MA, USA) sensor during April 2014.

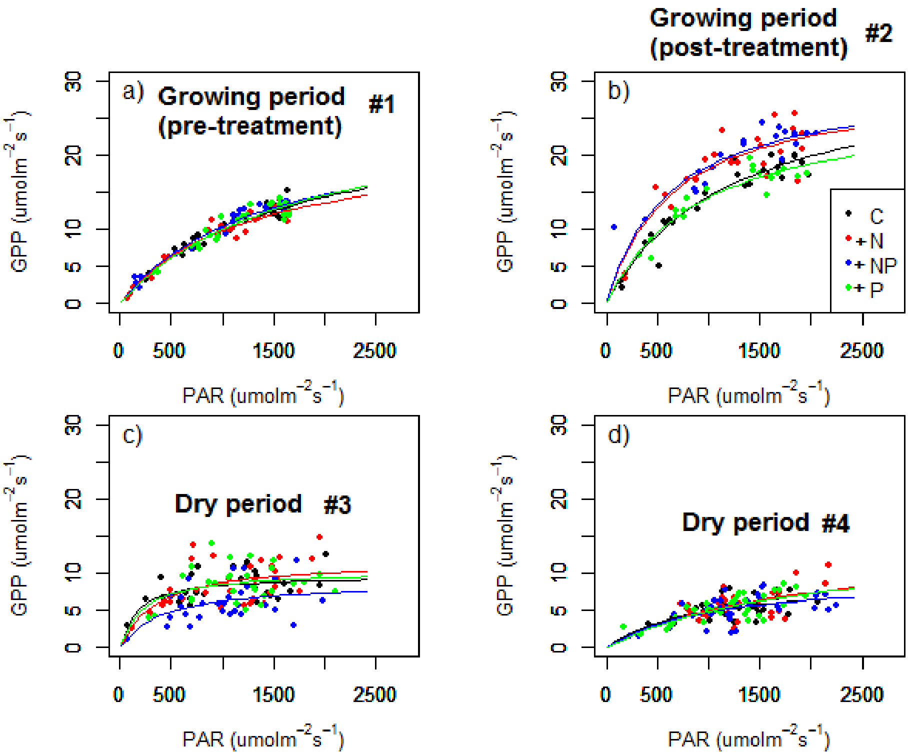

Figure 2. Photosynthetic light response curves derived for each growing period: **(a)** pre-treatment and **(b)** post-treatment and drying periods (**c** and **d**). Treatments are presented in different colors. Lines represent the Michaelis–Menten function fitting gross photosynthesis (GPP, µmol CO_2 m^{-2} s^{-1}) and photosynthetic active radiation (PAR, µmol m^{-2} s^{-1}).

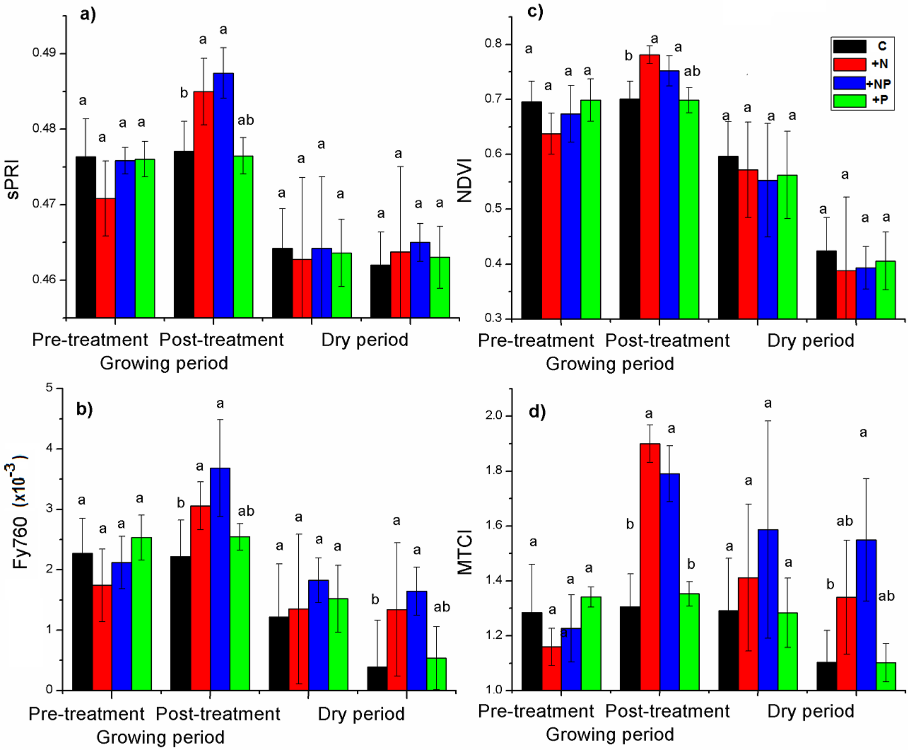

Figure 3. Seasonal time course of mean midday physiologically-driven vegetation indices; **(a)** scale photochemical reflectance index, sPRI **(b)** apparent fluorescence yield (Fy760), and structure-driven vegetation indices, **(c)** NDVI, and **(d)** MTCI among C, N, NP and P treatments in a Mediterranean grassland in Spain. Bars indicate ± standard deviation, $N = 4$. Different letters denote significant difference between treatments (Weilch t test, $P < 0.05$).

BGD
12, 11891–11934, 2015

Remote sensing-based model of photosynthesis

O. Perez-Priego et al.

Title Page
Abstract Introduction
Conclusions References
Tables Figures
◀◀ ▶▶
◀ ▶
Back Close
Full Screen / Esc
Printer-friendly Version
Interactive Discussion

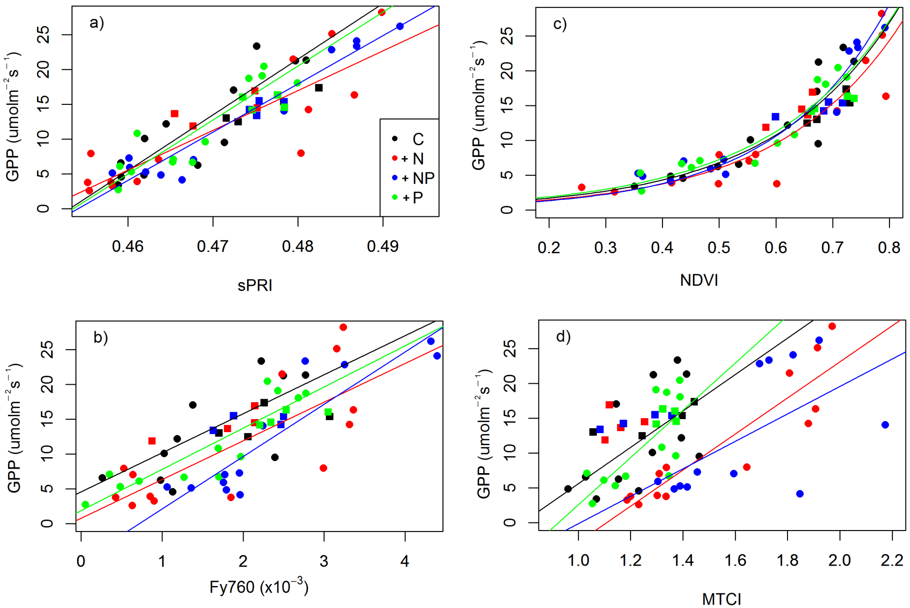

Figure 4. Relationship between GPP and remote sensing data: **(a)** scaled photochemical reflectance index (sPRI), **(b)** apparent fluorescence yield, **(c)** normalized difference vegetation index (NDVI), and **(d)** MTCI. Square symbols represent measurements taken in the pre-treatment (#1) and circles after fertilization (#2–#4). Data were obtained at midday and lines represent results from the regressions for each treatment excluding measurements in the pre-treatment.

BGD
12, 11891–11934, 2015

Remote sensing-based model of photosynthesis

O. Perez-Priego et al.

Title Page
Abstract | Introduction
Conclusions | References
Tables | Figures
◀| |▶
◀ ▶
Back | Close
Full Screen / Esc
Printer-friendly Version
Interactive Discussion

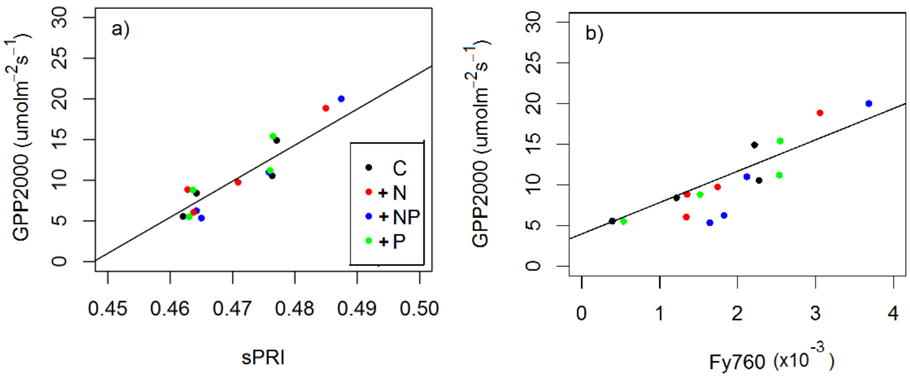

Figure 5. Relationship betweenGPP2000 and average values of sPRI **(a)** and apparent fluorescence yield (Fy760). Lines represent results the best linear regressions fitting the data.

BGD
12, 11891–11934, 2015

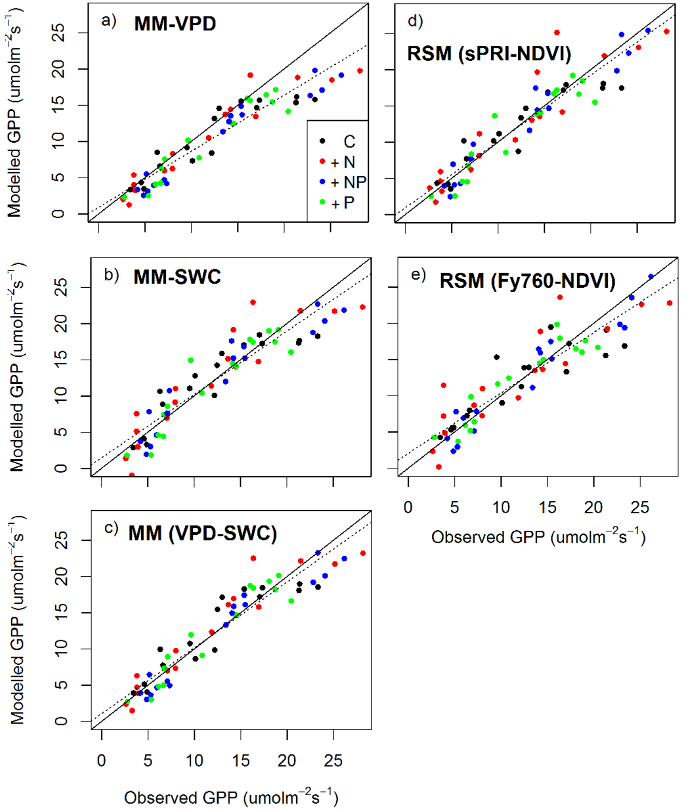

Figure 6. Comparison between measured GPP and GPP modeled with the best performing LUE model for each kind of formulation: MM (VPD, panel **a**), MM (SWC, panel **b**), MM (including VPD and SWC, panel **c**), RSM (sPRI-NDVI panel **d**), and RSM (Fy760-NDVI, panel **e**). Results from the cross validation analysis are presented in Table 3.

BGD
12, 11891–11934, 2015

Remote sensing-based model of photosynthesis

O. Perez-Priego et al.

Title Page
Abstract | Introduction
Conclusions | References
Tables | Figures
◂◂ | ▸▸
◂ | ▸
Back | Close
Full Screen / Esc
Printer-friendly Version
Interactive Discussion

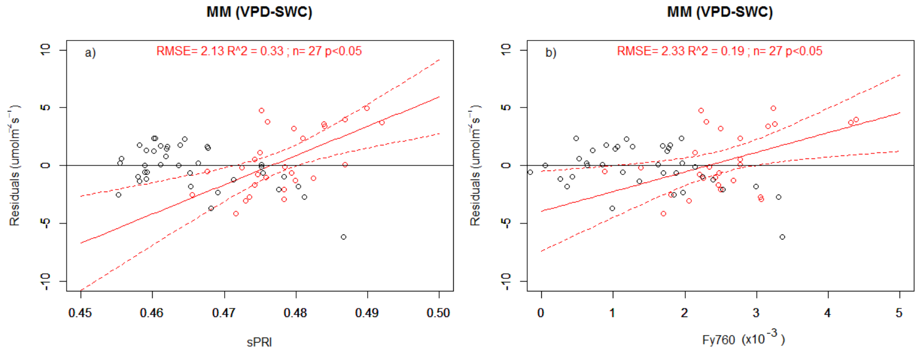

Figure 7. Correlation between residuals of the MM (VPD-SWC) model and **(a)** scaled photochemical reflectance index (sPRI) and **(b)** chlorophyll fluorescence yield (Fy760) taken from periods with high soil water content (SWC > 15 %, red circles). No correlation was observed when SWC < 15 % ($p > 0.5$, black circles).

BGD
12, 11891–11934, 2015

Title Page
Abstract | Introduction
Conclusions | References
Tables | Figures
Back | Close
Full Screen / Esc
Printer-friendly Version
Interactive Discussion

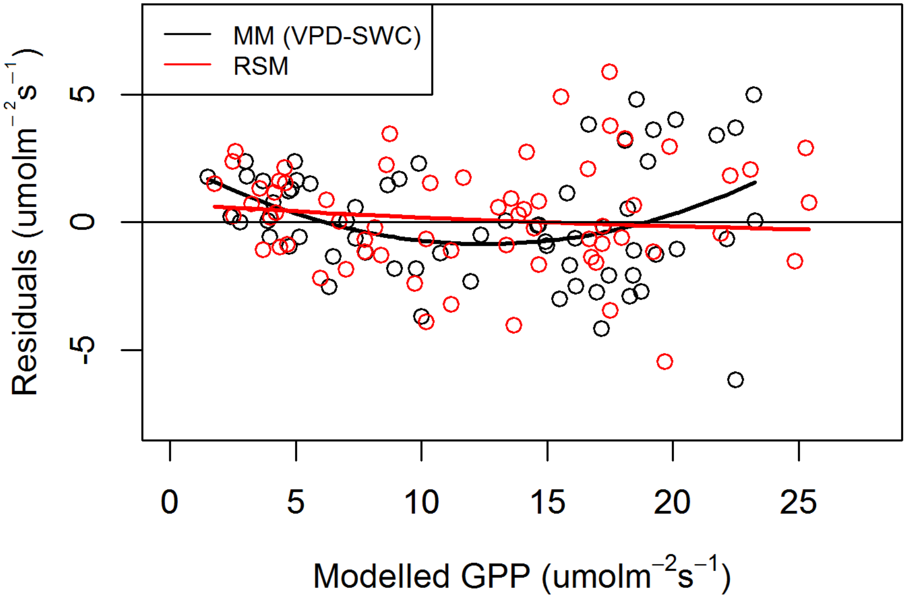

Figure 8. Plot between residuals of both the Meteo-driven model (MM-VPD) and Remote Sensing-based method (RSM) and modeled GPP values. Both lines represent the local polynomial regression fitting of the residuals against predicted values.

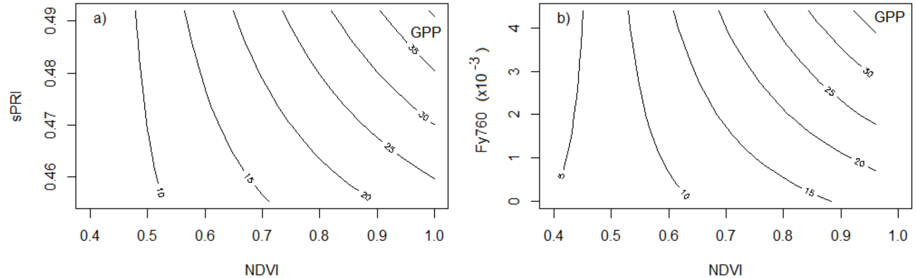

Figure 9. Contour plot indicating how variation in photosynthesis (GPP, µmol CO_2 m^{-2} s^{-1}) are explained by variations in the LUE and fPAR parameters of the RSM. While **(a)** sPRI and **(b)** Fy760 are indistinctly used as a proxy of LUE, the NDVI is taken as *f*PAR.

BGD
12, 11891–11934, 2015